ELSEVIER

Earth and Planetary Science Letters 202 (2002) 387–404

EPSL

www.elsevier.com/locate/epsl

Inverse modelling of elastic thickness by convolution method – the eastern Alps as a case example

Carla Braitenberg [a,*], Jörg Ebbing [b], Hans-Jürgen Götze [b]

[a] *Department of Earth Sciences, University of Trieste, Via Weiss 1, 34100 Trieste, Italy*

[b] *Institut für Geologische Wissenschaften, Geophysik, Freie Universität Berlin, Malteserstrasse 74-100, D-12249 Berlin, Germany*

Received 11 March 2002; received in revised form 7 June 2002; accepted 25 June 2002

Abstract

An unconventional scheme is used to estimate the flexural rigidity, or equivalently the elastic thickness of the lithosphere, given the topography and gravity data. The flexural rigidity is the parameter that governs the flexural response of the lithosphere in the frame of the thin plate flexure model. The scheme is an alternative to the widely used calculation of admittance of topography (sea-floor or continental topography) and gravity, bearing some advantages which are explained in the paper. The scheme involves the inversion of the gravity data in order to formulate a model of the crust–mantle interface (CMI) undulations. In a second step the flexure parameter is then evaluated from the relation between topography and CMI variations. Instead of calculating the admittance function using a spectral analysis, a set of point-load response functions are used in order to retrieve the optimal flexure parameter. This has two main advantages: instabilities of the numerical admittance evaluation at wavenumbers with low spectral energy in the topography are overcome and the analysis can be made over an area which is not necessarily rectangular, as required for the spectral analysis. The proposed method allows a higher space resolution of elastic thickness than any spectral method. For validation, the numerical strategy is applied to the situation of a realistic synthetic model, where all inputs and outputs are known a priori. Finally the spatial variations of the elastic thickness are studied in an area across the Eastern Alps.

Keywords: models; flexure; elastic properties; crust; mantle; isostasy; Eastern Alps

1. Introduction

The thin plate isostatic flexure model is a well-established modern formulation of the model of regional isostatic compensation. It has evolved from the isostatic model of Vening Meinesz [1], who first quantified the flexure model of isostasy. The model describes the lithospheric or oceanic lithosphere as an elastic thin plate that flexes elastically in response to external and internal loads. The outer loads are defined by the topography in continental areas, and by the bathymetry in oceanic areas. The inner loads are due to lateral density variations. Although being a relatively simple mathematical model, the predictions concerning the deformation due to loading and unloading have close agreement to the observations in diverse situations, as e.g. post-glacial rebound and

* Corresponding author. Tel.: +39-40-5582258; Fax: +39-40-575519.

E-mail address: berg@univ.trieste.it (C. Braitenberg).

0012-821X/02/$ – see front matter
PII: S0012-821X(02)00793-8

the loading of the oceanic crust due to submarine volcanoes. Further examples regard the study of orogenic belts and the evolution of sedimentary basins. For an exhaustive discussion of the different applications reference is made to the book by Watts [2], where a compendium of most of the existing literature on the subject can be found.

It is a key issue in the understanding of the structure and evolution of the lithosphere to determine the spatial variations of flexural rigidity or equivalently elastic thickness (T_e, see expression below relating the two). A compilation of 139 published T_e estimates in oceanic areas has shown that the flexural rigidity correlates well with the age of the lithosphere at the time of loading. The oceanic elastic thickness T_e, with values between 0 and 65 km, is approximately given by the depth to the 300–600° isotherm ([2], p. 241). A compilation of all existing 82 estimates of T_e in continental areas has found greater scatter of the values (0–130 km) and no simple dependency on load age ([2], p. 250). Instead it has been suggested that crustal composition is an important factor affecting T_e, as it controls the rheology and the geothermal gradient. Burov and Diament [3] developed an analytical and numerical approach to explain T_e in terms of the lithospheric rheology, thermal structure, and strain/stress distribution, allowing a means to constrain the lithospheric structure from estimates of T_e.

The retrieval of spatial variations of T_e has been made in the past either by working on a series of adjacent profiles (e.g. [4], for continents; [5] for oceans), or on a mosaic of rectangular areas (e.g. [6] for continents; [7], for oceans), where for each profile or area one value of T_e is fitted. The modelling of flexure is accomplished either in the spectral domain or in the spatial domain. The data that are used in the calculations are generally the gravity field and the load given by both the topography or bathymetry and the crustal density inhomogeneities. In the spectral domain the admittance and coherence of the load and the gravity field is determined.

The admittance $Z(k)$ is computed from the spectra and the cross-spectra of the gravity and topography at wavenumbers k with (e.g. [8]):

$$Z(k) = \frac{|\langle B(\vec{k}) H(\vec{k})^* \rangle|}{\langle H(\vec{k}) H(\vec{k})^* \rangle} \tag{1}$$

where $H(\vec{k})$ and $B(\vec{k})$ are the Fourier transforms (FT) of the topography and the gravity, respectively, $\vec{k} = (k_x, k_y) = 2\pi(v_x, v_y)$ is the two-dimensional wavenumber, v_x and v_y are the spatial frequencies along the x- and y-axis. The brackets indicate averaging over annuli of width dk, and * stands for complex conjugate.

The coherence $Q(k)$ is computed in a similar manner by:

$$Q(k) = \frac{\langle B(\vec{k}) H(\vec{k})^* \rangle^2}{\langle H(\vec{k}) H(\vec{k})^* \rangle \langle B(\vec{k}) B(\vec{k})^* \rangle} \tag{2}$$

A discussion on the different flavors of calculating these expressions can be found in McKenzie and Fairhead [9] and Banks et al. [10]. The admittance and coherence analysis suffer from several common problems. The first is the poor stability of the estimated values in case of small topographic load, as the spectral values enter the calculations in the denominator and can lead to numerical problems at wavenumbers at which the spectral coefficients are small; a further problem emerges in the case that spatial variations of the elastic thickness are present in the investigated structure. The expected flexure admittance curves, defined in major detail below, require a high spectral resolution and consequently spatial extensions of the analyzed window of at least several hundred kilometers in one direction. Higher spatial resolution can be achieved by using the maximum entropy spectral evaluation [6], but it remains intrinsically limited. Consequently also the inverted elastic thickness values represent an average over a large area and spatial variations are difficult to retrieve. Another handicap is due to the fact that the spectral analysis in 2D requires a square map of topography and gravity data availability, which is sometimes not available due to geographical reasons. The consequence of this can be a substantial geographical reduction of the studied area, due to a trimming to a rectangular area.

In the spatial domain the flexure due to the

load can be solved using finite element (FE), analogous numerical methods or analytical models (e.g. [11,4]). Another methodology consists in finding the expression of the deformation of the elastic plate due to a point load. The flexure due to an arbitrarily shaped distributed load can then be calculated from the convolution of the point-load response function with the load. This procedure was followed by Watts et al. [12], who obtain the radial response function from a series expansion around the origin of the deflection due to a point load centered in the origin. The method has been pursued successively by Cazenave et al. [13] and applied in oceanic areas (e.g. [5,7]). The retrieval of T_e in these works is done by fitting the gravity field produced by the load and the flexed lithosphere to the observed gravity field. The flexure is evaluated for different values of T_e and the modelled gravity field is calculated for each case, until a satisfying agreement between the model and the observations has been found.

If available, additional geophysical constraints can be used in the modelling. Canales and Danobeitia [14] use seismic lines to constrain the amplitude of a subsurface load, comparing the observed basement depth with the predictions from the flexure model.

In the present paper a scheme is proposed in which different aspects of the above practices are merged. The lithosphere is assumed to deform elastically in response to sufficiently old loads ($>10^6$ yr) according to the thin plate model. The flexural rigidity of the lithosphere is allowed to vary spatially. The lithosphere is allowed to have density variations that are considered as internal loads and added to the external topographic or bathymetric load. The flexure modelling is accomplished in the spatial domain in a manner similar to the one proposed by Watts et al. [12], and the T_e is modelled in 2D. The methodology involves the convolution of the load with the response functions of the elastic plate model to a point load, obtaining the model flexure. The response functions are calculated through the 2D inverse FT of the flexure filter function defined below. The model flexure is compared to the observed flexure of the lithosphere, which is assumed to be equal to the CMI undulations, which are obtained by constrained gravity inversion or forward modelling. All geophysical constraints regarding structure or geological models, from which density variations can be estimated, are taken into account in order to obtain a model of the CMI undulations by inversion or forward modelling of the observed gravity data.

In the following the above problems are illustrated with some practical examples. First the situation of a synthetic flexure model is constructed, where all parameters can be controlled and different cases tested. Then the method is applied to the Eastern Alpine area, taking advantage of an existing 3D density model, formulated by constrained gravity inversion and forward modelling.

2. The thin plate elastic model

For a homogeneous isotropic elastic thin plate, such as the lithosphere at large scale, the flexure $w(x, y)$ of the plate loaded by a load $h(x, y)$, in frequency space is defined by the transfer function $F(\vec{k})$ (e.g. [2,15,26]):

$$W(\vec{k}) = F(\vec{k})H(\vec{k}) = \frac{\rho_l}{\rho_m - \rho_{infill} + \frac{D}{g}|\vec{k}|^4} H(\vec{k}) \tag{3}$$

where $W(\vec{k})$ is the FT of the flexure $w(\vec{r})$ of the plate, $H(\vec{k})$ is the FT of the load, ρ_m, ρ_{infill}, ρ_l are the densities of the mantle, of the material filling the flexural depression, and the load, respectively, g is the normal gravity. $\vec{r} = (x, y)$ is the space-vector, $\vec{k} = (k_x, k_y) = 2\pi(v_x, v_y)$ is the two-dimensional wavenumber, v_x and v_y are the spatial frequencies along the x- and y-axis, respectively, and D is the flexural rigidity of the plate, which is a function of Young's modulus E, the Poisson ratio σ, and the equivalent elastic thickness T_e as:

$$D = \frac{ET_e^3}{12(1-\sigma^2)} \tag{4}$$

In the paper we refer to the elastic thickness instead of to the flexural rigidity. We adopt stan-

dard values for the parameters that allow to express elastic thickness in terms of flexural rigidity, with $E=10^{11}$ Pa and $\sigma=0.25$. The elastic thickness must be scaled accordingly for a different choice of the rheological model.

In the thin plate flexure model it is generally assumed that the flexure $w(\vec{r})$ approximately equals the deviations from the flatness of the CMI. Therefore Eq. 3 gives the linear relation $F(\vec{k})$ between the FTs of the sum of the topographic and subsurface loads and the CMI undulations. $F(\vec{k})$ is characteristic of the elastic thickness of the thin plate.

For the case of an inhomogeneous plate, $F(\vec{k})$ is dependent on position $\vec{r}$. The load is given by the sum of the subsurface and surface load, the latter being given by surface topography in continental areas, by ocean floor topography in oceanic areas.

3. Flexure and the gravity field

As mentioned above, the modelling of the flexure is frequently done assuming the load and the gravity field (e.g. [6,10]), instead of assuming the undulations of the CMI, because of difficulties in retrieving broad areas mapped by seismic imaging of the CMI undulations.

The gravity field of the flexed lithosphere can be approximated by the gravity contribution of the CMI flexure, as at the CMI the greatest density jump occurs. The gravity effect can be evaluated by a series expansion of the FT of the n-power of $w(\vec{r})$ [16]:

$$\mathrm{FT}[\Delta g(\vec{r})] = -2\pi G(\rho_m-\rho_c)e^{-|\vec{k}|d}\sum_{n=1}^{\infty}\frac{|\vec{k}|^{n-1}}{n!}\mathrm{FT}[w^n(\vec{r})] \quad (5a)$$

with $\Delta g_m(\vec{r})$ denoting the gravity field produced by the CMI, d the average depth of the CMI, and G the universal gravity constant. ρ_c is the crustal density, and all remaining variables are as in previous equations. d is measured from the zero height level. A further approximation is then made, and the series expansion is truncated at the first term ($n=1$), in order to obtain a linear relation between the FT of the flexure and the gravity field:

$$\mathrm{FT}[\Delta g_m(\vec{r})] = -2\pi G(\rho_m-\rho_c)e^{-|\vec{k}|d}W(\vec{k}) \quad (5b)$$

This, together with Eq. 3 gives:

$$\mathrm{FT}[\Delta g_m(\vec{r})] = \frac{-2\pi G(\rho_m-\rho_c)e^{-|\vec{k}|d}}{\rho_m-\rho_{infill}+\frac{D}{g}|\vec{k}|^4}\rho_1 H(\vec{k}) \quad (5c)$$

Once again the transfer function relating the topography and the gravity is linear, and the relevant parameters can be determined by fitting the experimental admittance or coherence (see Eqs. 1 and 2). This has been done extensively in many publications (e.g. [15]).

There exist several problems inherent in using this broadly used method of determining the flexure parameter D. The first problem is connected to the fact that the above expression is from an approximation: it defines the gravity field caused by an infinitely thin flat sheet of surface density σ:

$$\sigma(\vec{r}) = 2\pi(\rho_m-\rho_c)w(\vec{r}) \quad (6)$$

lying at the depth d. For a downward-flexed plate, the gravity field will always be overestimated by Eq. 5b, as is proved in the Appendix. This fact is illustrated in Fig. 1, where the upward-continued field and the analytical field of a synthetic crustal root (density contrast -500 kg m^{-3}) is calculated: the energy of the upward-continued field is about 20% greater than the energy of the correct field. Consequently the elastic thickness is in danger of being overestimated: from the observed gravity data, it is interpreted by a plate which flexes less than it should do to produce the given gravity effect, and thus it is stiffer.

One way to overcome this problem is to calculate the flexure for different flexure parameters,

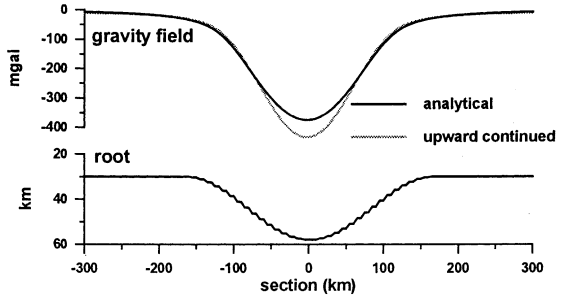

Fig. 1. Upward-continued and analytical gravity field versus section (along x or y) for a synthetic crustal root.

and for each case evaluate the gravity field by the Parker series expansion. The calculated gravity field is then best fitted to the observed field. This procedure has been made e.g. by Calmant [5] for the study of flexure in oceanic areas.

Another analysis scheme, which we pursue, separates the modelling of the CMI from the flexure analysis. In a first step, the CMI undulations are inverted by analyzing the long-wavelength component of the observed gravity field. Results from seismic investigations may be used to constrain the CMI solution. The solution may also be improved by modelling the upper crustal structures, taking sedimentary basins or other evident features known from geological investigations into account. These are important structures in the flexure analysis, as they not only affect the gravity field, but also the load. This can be done e.g. by using the iterative hybrid spectral-classical inversion method which has already been extensively tested on synthetic models [17] and in various geographical areas as Alps [18,19], Tibet [20,21]) and Karakorum [22]. In a second step, the relation between topography and CMI signals is investigated in order to find the flexure parameters.

4. Describing and testing the method of flexure convolution analysis

The classical method for admittance and coherence computation is based on the evaluation of the 2D FTs of both gravity and topography grids, and then of the ratio of the respective spectra. As directional isotropy of admittance is generally assumed, at each resolved wavenumber, the spectral coefficients are averaged over all azimuthal directions. Some drawbacks come along with this spectral approach. The first one is that it involves an averaging process over the entire grid used in the spectral evaluation. Spatial variations in elastic thickness may consequently be retrieved only to a limited extent. The second problem is due to the fact that the ratio goes to infinity when the spectral coefficients of the topography go to zero, as they appear in the denominator. Alternatively the calculation can be operated in space domain, and involves convolution of the topography grid with the flexural response to a point load. In the sequel, this flexural response function is called the impulse response of the filter as it is associated to the flexure process. The filter function $F(\vec{k})$ for flexure (Eq. 3) is radially symmetric, as well as the impulse response. The impulse response functions are obtained numerically by the inverse FTs of the transfer function $F(\vec{k})$, which relates topography to flexure in frequency space. The numerical calculation of the response functions requires some attention regarding the frequency resolution and the Nyquist frequency adopted in the inverse FT. The choice of the parameters (size of grid N, Nyquist frequency f_N) of the spectral grid with the values of the transfer function is motivated by

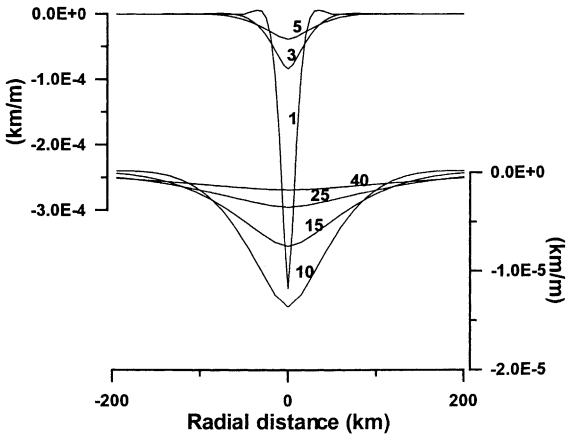

Fig. 2. Response of flexure to a point load for different values of the elastic thickness. The vertical axis on the left corresponds to $T_e = 1$, 3 and 5 km, the T_e axis on the right is for 10, 15, 25, 40 km.

two conditions: (1) the necessity of covering the filter function to sufficiently high-frequency components and with a sufficiently high frequency resolution, and (2) by the condition of obtaining the impulse response with a sampling interval comparable to that of the topography grid. The fulfillment of these conditions is limited by finite computer capacity, and a compromise must be made. The technical details on the calculation of the impulse response are reported in the Appendix. The impulse responses are plotted in Fig. 2, for values of elastic thickness from $T_e = 1$ km to $T_e = 40$ km, and parameters are defined in Table 1, synthetic model. As expected for a stiffer plate (greater T_e), the impulse response is smaller and decays more slowly with distance. For low T_e the response curves show a flexural bulge, and then decay to zero values toward greater distances.

5. Synthetic example

The method is tested in a controlled model situation, where all parameters which enter the computation are known. The flexure load is given by the topography of the Alpine arch and the lithospheric flexure is calculated adopting synthetic model T_e values. The T_e model with a resolution of 15 km is shown in Fig. 3A (kilometric axes in Gauss–Krüger projection). The 5-km resolution model of topography is shown in Fig. 3B. The synthetic CMI undulations (Fig. 3C) are obtained solving the flexure equations by finite difference. The calculations were kindly performed by Paul Wyer at Oxford University. Numerical values of model parameters from Eq. 3 are reported in Table 1.

The geographical dimensions of the CMI model are 550 km by 500 km, which are relatively small for the admittance/coherence analysis to be carried out, but do not present any problem of limitation for the convolution method. In order to test the stability of the method, we add noise to the data of our synthetic flexure CMI. This noise is Gaussian and its standard deviation is 5% percent of the maximum excursion of the CMI undulation. Different percentage values were tested, and it was found that values greater than 5% mask the CMI undulations too much, and are unrealistic. In fact, already the 5% value masks the CMI undulations considerably, as can be observed in Fig. 3D. The topography and the synthetic flexure CMI are the input to the flexure analysis by the convolution method. The impulse flexure response curves that are convolved with the topography comprise the entire set from $T_e = 0$ km to $T_e = 25$ km, with a step of 0.5 km. The flexure analysis is carried out on square overlapping windows of the studied area. On each window the root mean square (rms) of the difference between the flexure CMI obtained for a specific T_e and the model CMI undulations is determined. The inverted T_e for the specific window is the one that minimizes the rms error. Different sizes of the windows were tested, the shift of each window being held at 15 km. The inverted T_e field is thus obtained with a spacing of 15 km, and every value was obtained by a best-fit approximation of the model CMI on a window of a certain size. The window size was allowed to vary between 60 and 170 km, and the resulting

Table 1
Parameters used for the computation of the flexure curves, both for the synthetic case and the Eastern Alps

		Synthetic model	Eastern Alps
Mantle density	ρ_m	3.1×10^3 kg m^{-3}	3.3×10^3 kg m^{-3}
Load density	ρ_l	2.7×10^3 kg m^{-3}	2.67×10^3 kg m^{-3}
Infill density	ρ_{infill}	2.7×10^3 kg m^{-3}	2.8×10^3 kg m^{-3}
Young modulus	E	10^{11} Pa	10^{11} Pa
Poisson ratio	σ	0.25	0.25
Grid spacing	dx, dy	5 km	5 km
Grid size CMI	L_x, L_y	550 km by 500 km	400 km by 270 km
Grid size topo	L_x, L_y	1200 km by 1200 km	1200 km by 1200 km

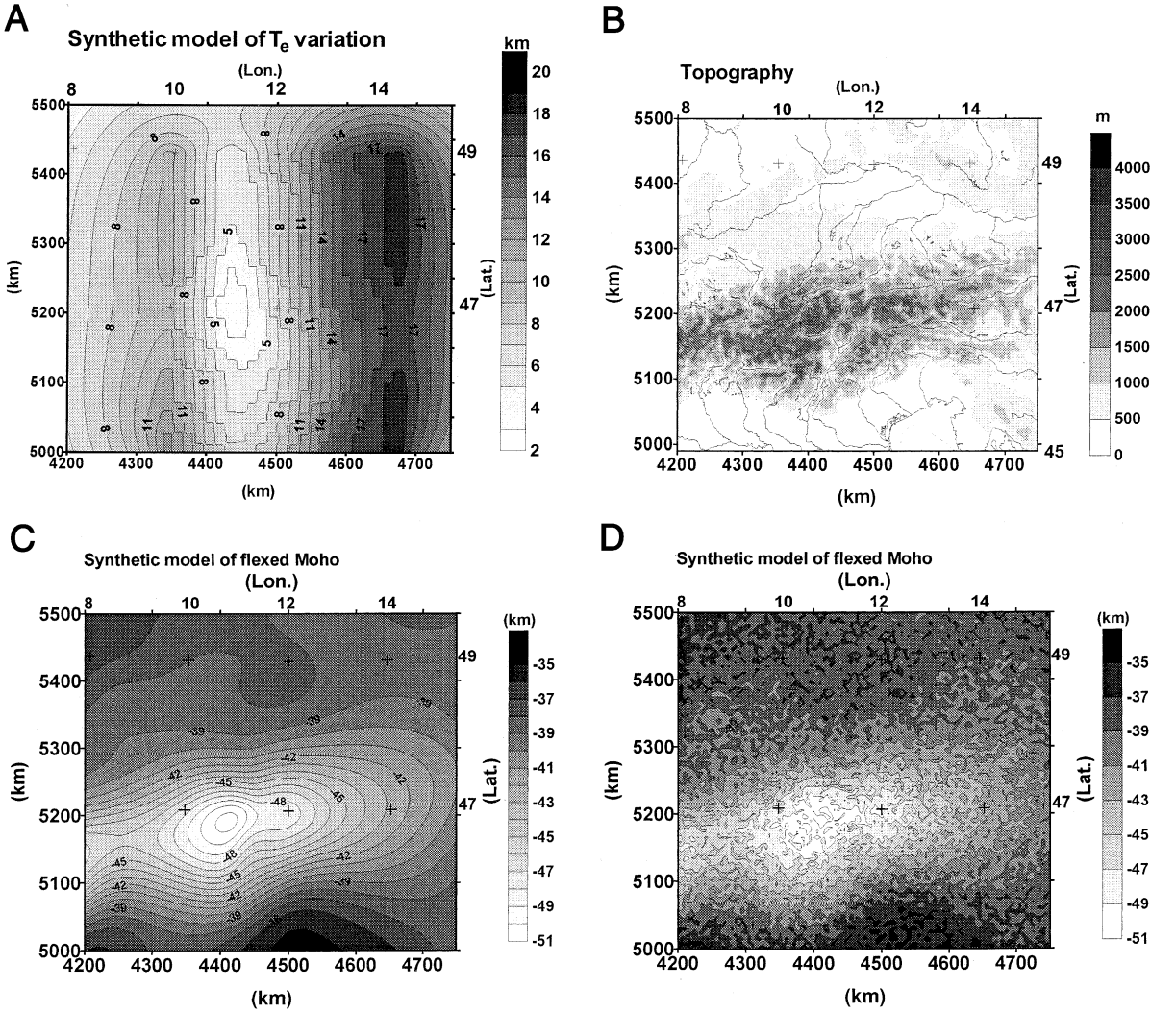

Fig. 3. Maps of the synthetic model. (A) The model elastic thickness (in km). (B) The Eastern Alpine topography (in m). Topography by the US Geological Survey GTOPO30-grid. (C) The resulting synthetic flexure CMI (in km). (D) The resulting flexure CMI (in km) in presence of random Gaussian noise in the data.

inverted T_e field was compared to the input T_e field. Increasing the window size enhances the numerical stability in the statistical evaluation. In the case of the CMI with no additional noise, the T_e values are retrieved with a rms error of 0.9 km, with a window size of 90 km. Increasing the window size does not reduce the evaluation error considerably. In presence of noise, the T_e values are retrieved with a rms error of 1.3 km considering a window size of 135 km. A further increase of the window size reduces the evaluation error by a small amount (0.1 km). A summary of the test is given in Table 2, where rms difference between the inverted T_e grid and the model T_e grid is given for different window sizes (60–170 km). The calculated flexure is plotted on Fig. 4A,B for the case of noise-free CMI and 5% noise, respectively. One can see that the model T_e is retrieved well, even in the case of high noise, as for the second case (Fig. 4B).

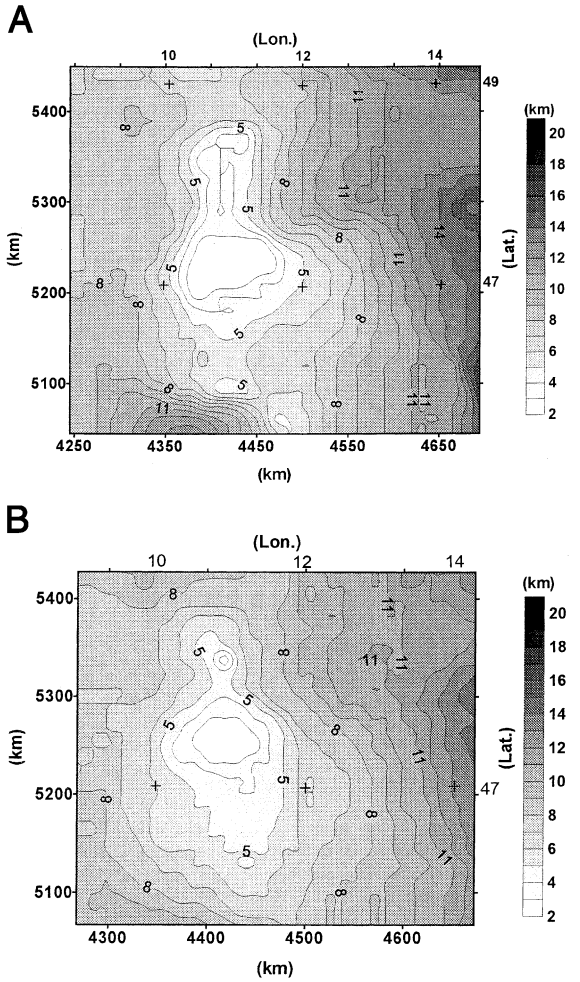

Fig. 4. Map of the fitted values of elastic thickness for: (A) noise-free synthetic CMI undulations, and (B) synthetic CMI undulations with Gaussian noise.

6. The spatial variations of T_e in the Eastern Alps

The numerical strategy to retrieve the spatial variations of T_e is now applied to the Eastern Alps, using a model of the CMI undulations and of the surface and crustal loads. We use the results from a detailed study [23] that was concerned with the interpretation of the observed gravity data in a geographic area of 400 km by 300 km extension centered on the recent TRANSALP profile (TRANSALP Working Group [27]). The crustal density model is presently the most detailed available for the Eastern Alps, and is constrained by both geological and geophysical information. Small differences to the results presented by Ebbing et al. [23] are due to inclusion of recent gravity measurements and ongoing investigations.

The Alps are an orogenic belt extending from the French-Mediterranean area to Switzerland and Austria. The present geologic structure is the result of several tectonic processes, which include both extensional and compressional strain regimes, subduction of oceanic crust and collision of continental blocks due to plate motions [28]. Airy-type local compensation isostatic models that exclusively take the topographic load into account failed to explain the crustal structure, as the observed crustal thickness is greater than that according to these models. Furthermore the greatest elevation of topography falls North of the observed Bouguer gravity minimum value across the Alpine range, a further indication of the presence of buried loads (e.g. [18,29–31]). The investigation of the isostatic equilibrium according to the lith-

Table 2
Dependence of quality of T_e evaluation on size of analysis windows during process of inversion for the synthetic case

Window size (km)	Rms on T_e CMI without added noise (km)	Rms on T_e CMI with added noise (km)
60	0.96	2.7
75	0.93	2.0
90	0.86	1.6
105	0.87	1.5
120	0.81	1.3
135	0.84	1.3
150	0.79	1.2
165	0.82	1.2
170	0.80	1.2

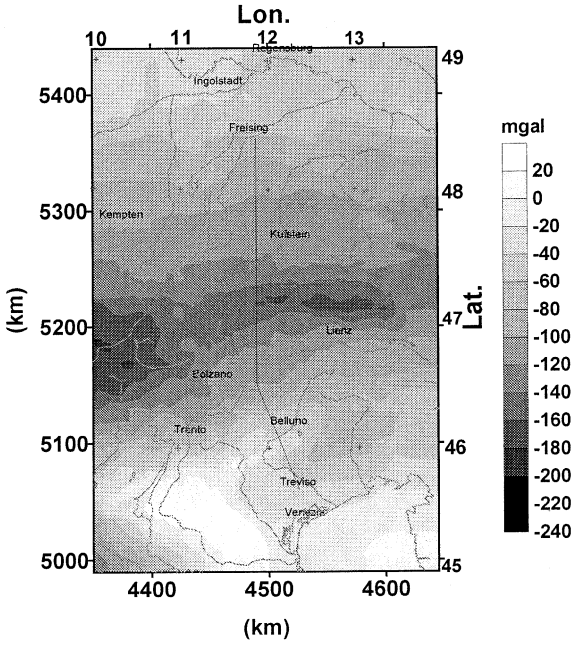

Fig. 5. Map of the observed Bouger gravity field in the Eastern Alps. Data courtesy of B.G.I. (Toulouse), G.G.A. (Hannover) and University of Vienna. Black line shows position of TRANSALP profile.

ospheric flexure models has been done in the Eastern Alps by several authors, but exclusively along profiles [4,32–34]. These studies were done using different approaches, including forward modelling of the gravity field with the use of flexure models [4,32,33], and the forward modelling of the curvature of the basement in the area of the foreland basin [34]. Also these studies found that the subsurface loads must give a relevant contribution to the total load. An improvement of our study with respect to these studies is that now a detailed model of the crustal loads is available in the Eastern Alps. Therefore the modelling of the spatial variations of T_e can be fulfilled independently from the modelling of the crustal loads, which otherwise must be modelled in the course of the flexure modelling. Details on the results of the above studies will be given in the discussion of the results.

Ebbing et al. [23] followed two approaches of gravity interpretation, the first being a combination of 3D forward modelling and gravity inversion, the second a pure 3D modelling. The models presented there were based on results of older seismic studies and the recent TRANSALP profile (TRANSALP Working Group [27]). Geologic and tectonic information served as additional model constraints for near-surface structures, which enabled a detailed analysis especially of the mass distribution within the uppermost 10 km of the crust.

The inversion approach is representative of a case in which only the surface structure may be forward modelled, because the lack of information from deep seismic sounding does not allow a full 3D modelling of the crust. The full 3D model relies in its deep part strongly on the results from seismic studies, and is representative of a case where these are available.

The goal of the flexure analysis is to determine to what extent the structural model is compatible with the flexural isostasy model and what the spatial variations of T_e are. As shown by various studies before, the calculation of the flexural rigidity requires the consideration of buried loads to avoid unreasonable results [2,10]. The use of a well-defined density model provides a means to

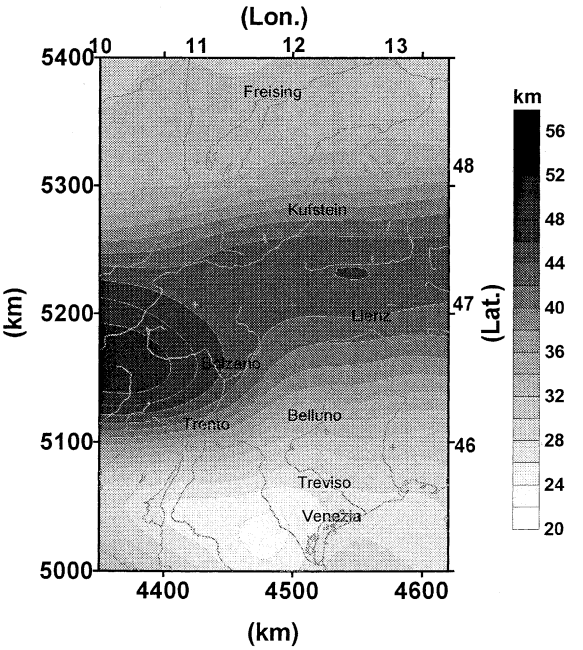

Fig. 6. Map of the CMI undulations according to the gravity inversion in the Eastern Alps.

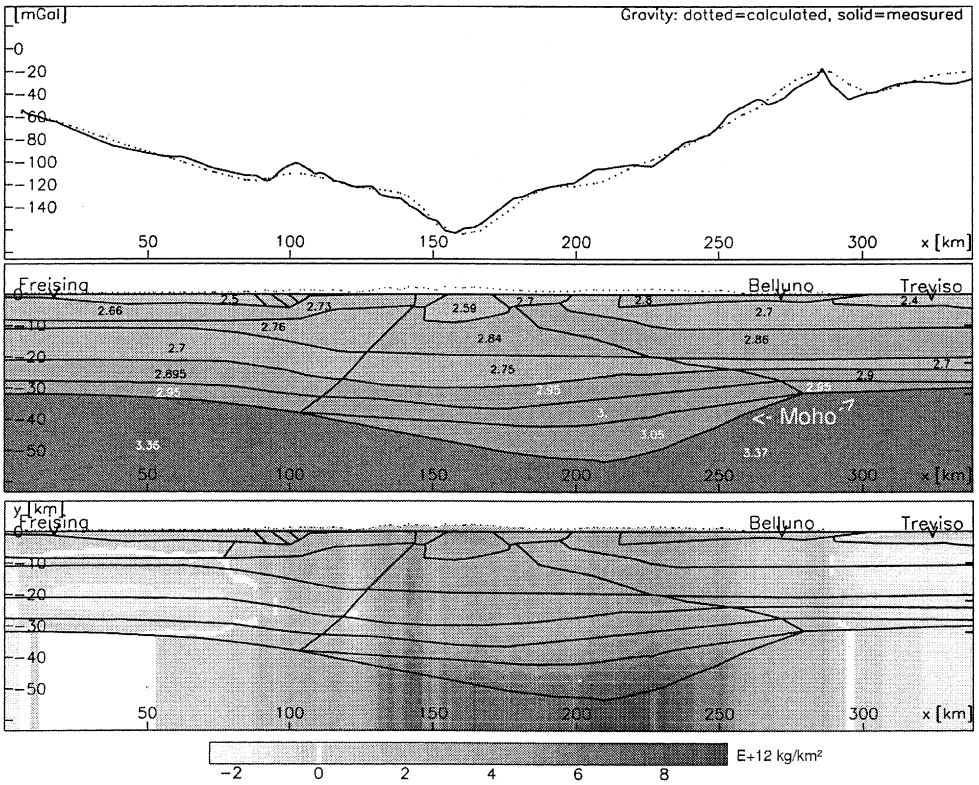

Fig. 7. Section along the TRANSALP profile through the forward crustal model (for geographical position of the profile see Fig. 5). Top: modelled (dotted) and observed (solid) Bouguer gravity. Center: density model, densities in 10^3 kg m^{-3}. Bottom: load distribution of the model relative to a crustal reference density of 2.8×10^3 kg m^{-3}.

quantify these buried loads and to include them into the analysis of flexural isostasy.

7. The spatial variations of T_e in the Eastern Alps

In Fig. 5 the terrain-corrected Bouguer gravity field over the studied area is plotted. For the gravity inversion, the Bouguer field was stripped from the contribution of the upper 10 km of the crust, low-pass filtered with cut-off period of 75 km, and the CMI undulations shown in Fig. 6 were obtained. The complete 3D crustal forward modelling (a section of which is presented in Fig. 7) resulted in the CMI undulations plotted in Fig. 8. The greatest differences between the two models of the CMI undulations are due to the steep gradients that characterize the forward model in the southern border of the Alpine arch and that a priori cannot be reproduced in the process of inversion, as wavelengths smaller than 75 km variations are not considered.

As in the case of the synthetic model, the load and the CMI undulations are the input data to the flexure analysis. The load is given by the sum of the topographic load and the inner-crustal loads. The topographic load is equal to the product of the topographic height and the density of 2670 kg m^{-3}, the same as used for the topographic reduction.

The calculation of the inner-crustal loads is done in vertical columns:

$$L_{\text{buried}} = \sum_{i=1}^{N} h_i \rho_i - \sum_{i=1}^{N} h_i \rho_c$$

with L_{buried} inner-crustal loads, h_i thickness of the i-th layer, ρ_i density of the i-th layer and ρ_c the

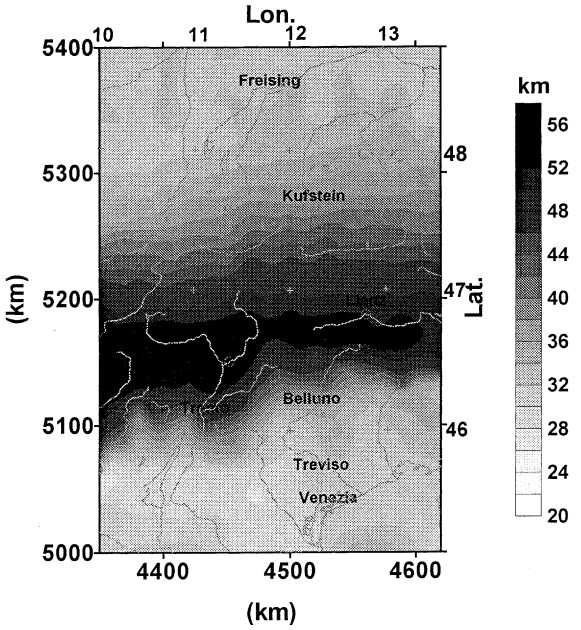

Fig. 8. Map of the CMI undulations in the Eastern Alps according to the gravity forward modelling.

density of the reference crust. In our model the crustal reference density is equal to 2800 kg m^{-3}, the mean crustal density of the forward density model.

A plot of the total crustal load, obtained from the sum of the topographic and subsurface loads is made in Fig. 7. Inner and topographic loads contribute in approximately equal amount to the total load.

The best-fitting T_e value is deduced from the minimum of the rms difference between the observed and computed CMI undulations. The analysis is carried out on square windows of 105-km sides, which are shifted by 15 km in order to cover the entire investigated area. The size of the window was selected according to the results found in the preceding paragraph on the inversion of T_e in the synthetic model.

First, the CMI undulations obtained from gravity inversion were analyzed. Here, the inner loads refer to crustal inhomogeneities down to a depth of 10 km, as below a homogeneous crust was assumed. The resulting spatial variations of T_e are plotted in Fig. 9A, the residual CMI undulations (flexure CMI minus gravity CMI) in Fig. 9B, and the resulting flexure CMI undulations in Fig. 9C.

The values of T_e are generally low, with a maximum value of 19 km in the northern part in correspondence of the Molasse Basin. The mountainous area has lower values between 3 and 9 km. An area of locally higher T_e values is found SE of the town of Bolzano. The misfit in CMI undulations is highest in the southwestern part of the investigated area and along the axis where the CMI is deepest, W and NNE of the town of Bolzano.

We now compare this result with that given by the aid of the 3D forward model of the complete crustal structure. The convolution analysis was made again on square windows of 105-km sides, shifted by 15 km. As before, the load (topographic and inner-crustal) was convolved with the flexure response functions, in order to obtain the modelled flexure CMI. The load now comprises the crustal density inhomogeneities of the entire crust, not only those limited to the upper 10 km, as in the previous case. The model T_e, the CMI residual and the flexure CMI undulations are plotted in Fig. 10A–C, respectively. Again the T_e values are generally low, with highest values found in the NE of the investigated area. The main body of the Alpine range has values around 1–3 km. The residuals are altogether low, in the order of 2–3 km, except in the southern part, in correspondence with the Vicenza gravity high and in the area where the CMI reaches its deepest values (area southeast and northwest of the town of Bolzano). Altogether the residuals are smaller in the latter case of the fully modelled crust.

8. Discussion of the observed spatial variation of T_e values in the Eastern Alps

The spatial variations of T_e that we have obtained for the Eastern Alps have a relatively high spatial resolution with respect to the previous studies, and are therefore not easily compared. We find an increase of T_e towards the Molasse Basin and in the south towards the Po Basin, whereas the main Alpine range is characterized by low T_e values. When considering crustal inho-

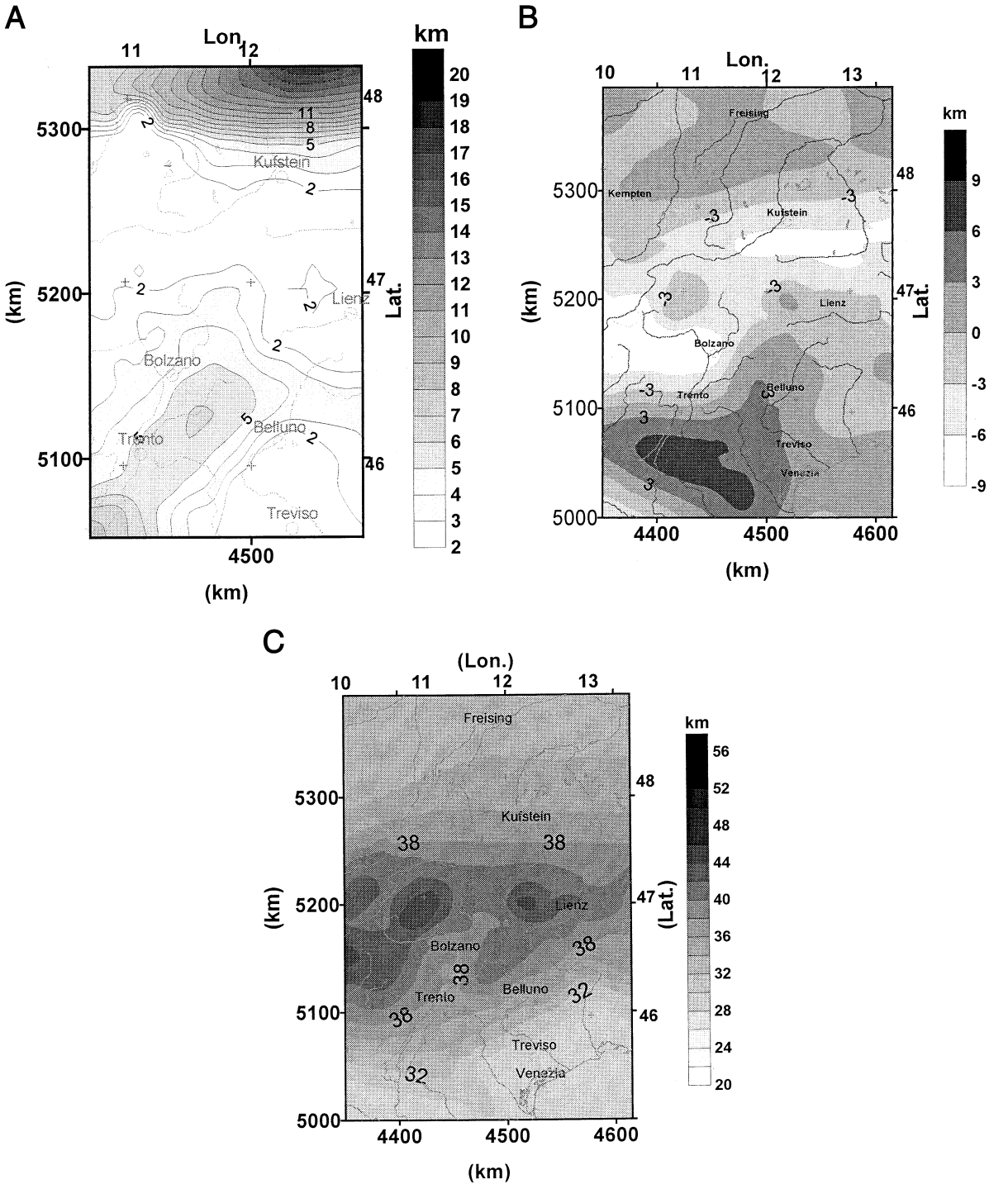

Fig. 9. Results from the flexure analysis of the CMI undulations as they resulted from the gravity inversion. (A) Spatial variations of T_e. (B) Residual of the CMI undulations (flexure CMI minus gravity CMI undulations). (C) CMI undulations predicted from the flexure model.

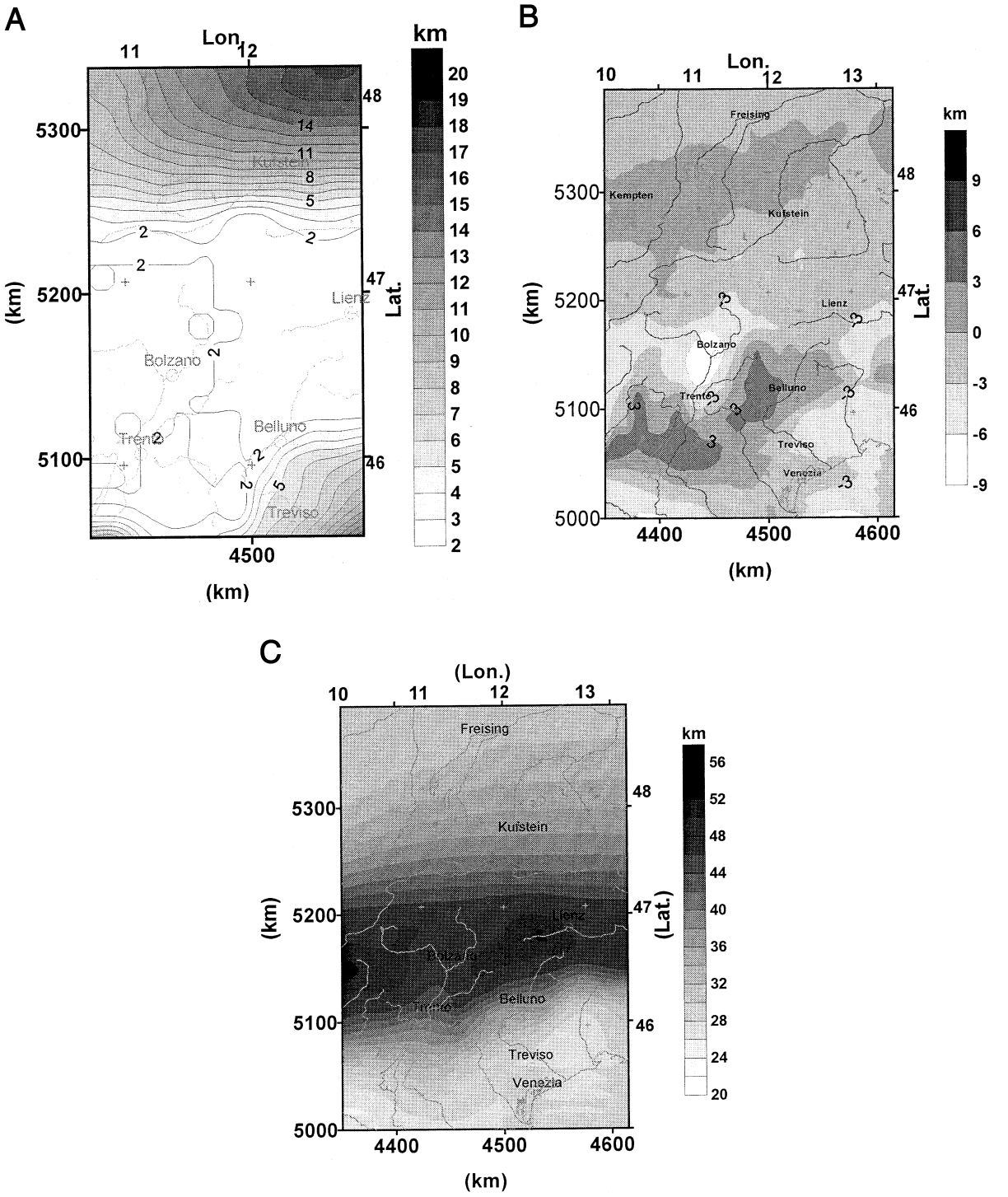

Fig. 10. Results from the flexure analysis of the CMI undulations as they resulted from the forwards gravity modelling. (A) Spatial variations of T_e. (B) Residual of the CMI undulations (flexure CMI minus gravity CMI undulations). (C) CMI undulations predicted from the flexure model.

mogeneity limited to a depth of 10 km, a higher T_e is found along the SW border of the Alpine range, correlated with the positive Bouguer values (compare Fig. 5). This increase of T_e values can be attributed to the lack of consideration of deep crustal loads. In fact, this area of increased T_e is not anymore present when the full crustal model is used for the inversion of the spatial variations of T_e.

The values of T_e we obtain in the Molasse Basin are comparable to those found by Stewart and Watts [4], who give a single value of 20 ± 5 km for a profile that crosses our study area, but extends about 400 km farther to the North. This profile replaced earlier results of Karner and Watts [32], who found a greater value of elastic thickness of 50 ± 5 km. The value found by Royden [33] is still higher (40 km for the Eastern Alps, 20 km for the Southern Alps), but was obtained by taking into account only the crustal loads of the sedimentary basins, and neglecting the influence of other density inhomogeneities, which could be the cause of this higher value. Finally, Andeweg and Cloetingh [34] modelled the basement depth of the German Molasse Basin along two profiles with a flexure model, obtaining a T_e value of 25 km. The low value of T_e we find in the central part of the Alpine range shows that here the crustal thickening conforms to that of a thin plate with low rigidity, near to an Airy-type local isostatic compensation. This could be an indication of the presence of a plate brake, which can be approximated as a continuous plate with a zone of low T_e values [2].

The high values of curvature of the CMI to the south of the Alpine crust cannot be modelled by the simple flexure model, and require a more sophisticated 3D mechanical model.

Another reason for the disagreement could be that horizontal and vertical tectonic forces linked to the collision process of the European and Adria plates must be taken into account, a task that can be only fulfilled in a complete 3D mechanical model.

9. Conclusions

In the present work a discussion on the use of spatial and spectral analysis of flexure is made. The spatial analysis refers to the convolution method for the flexure analysis, which requires the preparation of a series of unit impulse flexure response functions that convolved with the topographic load give the required thin plate flexure response. The correct flexure parameters are obtained by fitting the crustal structure, obtained from an independent geophysical investigation, with the thin plate flexure response to the load. This latter procedure bears two main advantages: the first is that the analyzed area can be of arbitrary shape, not necessarily square, a requirement necessary for the classical admittance/coherence analysis. A second advantage emerges in the case that the preponderant part of the load is topographic. In fact the analysis requires the load, i.e. the topography to be known over an extensive scale, which, depending on the elastic thickness involved, ranges from 200 to 1000 km in length. For a single T_e evaluation the crustal structure in terms of the flexed surface must be known on a much smaller scale, in other words on the order of 100 km length in order to obtain accurate values of the flexure parameters. This last condition is much less restrictive than in the case of the admittance analysis, where the size of the topography and of the gravity grids must be the same.

In the present work some aspects of the statistical evaluation of flexure parameters from the analysis of topographic and gravity data have been discussed. It has been pointed out that the widely used method of admittance/coherence analysis of topographic loads and gravity fields and subsequent interpretation with flexure admittance functions adopts only an approximated expression for the gravity field evaluation. The problem is more severe over those areas where the crust is thicker. This drawback is eliminated when the crustal structure is first determined by constrained gravity inversion and forward modelling, where corollary information can be built into the model. This information can be a geological and structural model, or results from seismic investigations. In a second step the flexure analysis is carried out.

The efficiency of the method has been tested in

the case of a synthetic model, where the flexure parameters of the lithosphere model were retrieved. The model topography corresponds to a section of the Alps, and the flexure parameters vary in plausible bounds. It has been shown that the method is robust. In presence of noise in the flexure CMI data, the method retrieved the right flexure properties. In the test, only surface topographic loads were considered, but the method can be extended analogously by adding subsurface loads into the lithospheric model.

This has been done in the real example of the Eastern Alps. The analysis of flexural rigidity was made taking advantage of a 3D density model, which allowed to quantify the buried loads across the mountain range and into the foreland basins. We find that the subsurface loads and the surface loads are correlated. This implies that the spectral flexure methods that retrieve the subsurface loads under the hypothesis of uncorrelated surface and subsurface loads cannot be applied in this area (e.g. [35]). The computation leads to results that have higher spatial resolution than previous studies. Regarding the northern foreland basin, our results for the values of T_e are comparable with previous studies, but we find a decrease of the values in the main Alpine range. As we used the continuous plate model with variable elastic thickness, this can be interpreted as the presence of a plate brake. The plate brake is to be expected as the Alps are at the border of two merging plates, the Eurasian and the Africa–Adria plate. Deviations of the modelled and the flexed CMI are probably due to recent tectonic forces, which can only be regarded by a 3D mechanical model.

In the near future, the same approach of flexure analysis will be carried out for the Andes and in the Tibetan area, by taking advantage of a recent model of the crustal structure computed from 3D forward modelling and inversion of the observed gravity field [20,21,36].

Acknowledgements

Prof. Maria Zadro is thanked for continuous assistance. Prof. Anthony B. Watts and his working group are thanked for discussions and calculating the synthetic undulations of the CMI. Dr. Sabine Schmidt provided important help concerning the density modelling software. The gravity data were received from Bureau Gravimetrique International (Toulouse), G.G.A. (Hannover) and Bruno Meurers (University of Vienna), which is thankfully acknowledged. We thank for the meticulous reviews of Prof. Gerhard Jentzsch and Dr. Gabriel Strykowski. The research has been supported by funds from the CNR, MUIR, DAAD, DFG-AZ: Go 380/19 and SFB 267, TP C6 and F4, and profited from a Sokrates/Erasmus teaching staff exchange program.*[AC]*

Appendix. Evaluation of the error in the approximate expression of the gravity field of the flexed plate

We may approximate the downward-flexed plate by a series of rectangular prisms of constant density and varying height. We then consider the error in the gravity calculation of a single prism, as for this latter case the error estimation can be computed analytically [24,25]. The gravity field caused by a prism of sides a, b, length L, and density $\rho_m-\rho_c$, the top of which is set at the depth d, is:

$$G_a(\vec{k}) = G(\rho_m-\rho_c)\,\mathrm{sinc}(k_x,\ a)\,\mathrm{sinc}(k_y,\ b)$$
$$(e^{-|\vec{k}|d}-e^{-|\vec{k}|(d+L)})\frac{2\pi}{|\vec{k}|} \qquad \text{(A1)}$$

with

$$\mathrm{sinc}(k_x,\ a) = \frac{\sin(k_x a/2)}{k_x/2}$$

The FT of the gravity field estimated by the upward continuation is given by:

$$G_u(\vec{k}) = 2\pi G(\rho_m-\rho_c)L\,\mathrm{sinc}(k_x,\ a)$$
$$\mathrm{sinc}(k_y,\ b)\,e^{-|\vec{k}|d} \qquad \text{(A2)}$$

We may consider the difference of these two spectra, normalized with the value of the spectrum at zero wavenumber (i.e. mean value component), that is:

$$G_a(0) = 2\pi G(\rho_m - \rho_c)abL \tag{A3}$$

The normalized difference is then:

$$\frac{G_u(\vec{k}) - G_a(\vec{k})}{G_a(0)} = \frac{1}{ab}\,\mathrm{sinc}(k_x,\ a)\ \mathrm{sinc}(k_y,\ b)$$

$$e^{-|\vec{k}|d}\left(1 + \frac{1}{L|\vec{k}|}(e^{-|\vec{k}|L} - 1)\right) \tag{A4}$$

Fig. 11A shows the normalized difference for different vertical extensions (L) of the prism and located at different depths d, the sides being $a = b = 20$ km, versus the spatial wavenumber k. It shows that the estimated coefficients $G_u(\overline{kk})$ of the gravity field are systematically greater than the correct ones $G_a(\vec{k})$ from the analytical expression, the relative error being greater for increasing vertical extension of the prism, for constant depth. The effect of this difference is illustrated on Fig. 11B, where the gravity values along a profile centered on and following parallel the direction of one side of the prism are shown. The two displayed cases correspond to (1) a prism of length 10 km with the top set at 5 km depth; and (2) a prism of 20 km length with top at 30 km depth. The black curves represent the correct field, the gray curves the upward-continued field. As the crustal root can be approximated by a set of vertical prisms, we conclude that the gravity effect calculated by the linear relation in Eq. 5b systematically overestimates the field produced by the root.

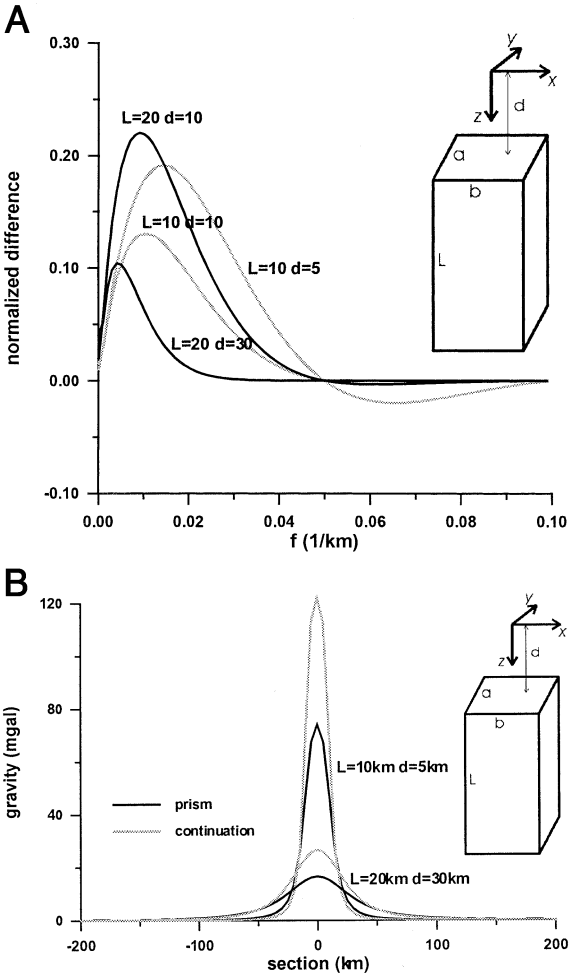

Fig. 11. Comparison of the upward-continued and analytical gravity fields. (A) Normalized upward-continued spectrum minus analytical spectrum versus radial frequency and for different prism lengths L and depths d (top of prism). (B) Upward-continued and analytical gravity field versus section (along x or y) for two prisms.

Technical details on the calculation of the flexure impulse response

The impulse response is obtained from the numerical inverse FT of the flexure transfer function. The flexure transfer function, a steadily decreasing function with maximum value in the origin, is calculated on a square grid of elements $N \times N$ and frequency resolution df. Due to the limited size of the spectral grid, the flexure transfer function must be truncated at a frequency f_0, which should be sufficiently small with respect to the value in the origin. For each elastic thickness a different value of N and df must be chosen, with d$f = 1/N$ dx. The choice of the parameters N and

Table 3
The maximum spatial frequency that must be covered by the grid (f_0 in Rm^{-1}), the sampling interval of the impulse response dr (in km), the number of elements along the baselength (N) of the square grid, and the minimum filter extension (R_{max} in km) required to reach percentage point 10% and 1% of the maximum value of the impulse response, for every elastic thickness T_e (in km)

T_e	f_0 (km^{-1})	Sampling dr (km)	N	R_{max}10 for percentage point 10% (km)	R_{max}1 for percentage point 1% (km)
1	4.00×10^{-2}	5	500	19	42
2	2.38×10^{-2}	5	841	33	68
5	1.20×10^{-2}	10	836	65	135
10	7.11×10^{-3}	15	938	105	230
20	4.23×10^{-3}	20	1183	180	400
30	3.12×10^{-3}	20	1604	245	520
40	2.51×10^{-3}	30	1326	310	650
50	2.13×10^{-3}	30	1568	360	760
60	1.85×10^{-3}	30	1798	400	870

Refers to the model parameters of the synthetic case.

df is to be made by the following conditions: dx = dy should be as close as possible to the sampling interval of topography; the spatial frequency f_0 for which the filter function has reached reasonably low values (1% of maximum value) should be less than the Nyquist frequency (df N/2); the transfer function should be evaluated with a reasonable frequency resolution (e.g. 1/100 of the maximum spatial frequency f_0 as defined above). An increase in the sampling interval dx implies that the values of the impulse response must be interpolated in order to apply the operation of convolution with topography. A lower maximum frequency f_0 and a lower frequency resolution df implies that the response functions are less well defined. In Table 3 the maximum frequency that must be covered by the grid (f_0 in km^{-1}), the sampling interval of the impulse response (dr in km), and the number of elements along the baselength (N) of the square grid, for each elastic thickness (T_e in km) are listed. It should be noted that the number of elements of the grid is N^2, and that this number rises quickly for increasing elastic thickness, as can be verified in the table. It has been thus necessary to increase the value of the sampling interval for greater elastic thicknesses, otherwise the grid is too large for the computer capacity.

When operating the convolution of the load, the filter function must be necessarily truncated at a certain distance (R_{max}), which determines the area over which the filter is convolved with topography. Again the criterion of considering all values greater than a certain percentage point of the maximum value is applied. In Table 3 the distances of the 1% and 10% percentage points are reported for different values of elastic thickness. In practice, the value of Rmax is conditioned by the data availability of topography covering the studied area.

References

[1] W.A. Heiskanen, F.A. Vening Meinesz, The Earth and Its Gravity Field, McGraw-Hill, New York, 1958, 470 pp.
[2] A.B. Watts, Isostasy and Flexure of the Lithosphere, Cambridge University Press, Cambridge, 2001, 458 pp.
[3] E.B. Burov, M. Diament, The effective elastic thickness (T_e) of continental lithosphere: what does it really mean?, J. Geophys. Res. 100 (1995) 3905–3927.
[4] J. Stewart, A.B. Watts, Gravity anomalies and spatial variations of flexural rigidity at mountain ranges, J. Geophys. Res. 102 (1997) 5327–5353.
[5] S. Calmant, The elastic thickness of the lithosphere in the Pacific Ocean, Earth Planet. Sci. Lett. 85 (1987) 277–288.
[6] A.R. Lowry, R.B. Smith, Flexural rigidity of the Basin and Range-Colorado Plateau-Rocky Mountain transition from coherence analysis of gravity and topography, J. Geophys. Res. 99 (1994) 20123–20140.
[7] S. Calmant, J. Francheteau, A. Cazenave, Elastic layer thickening with age of the oceanic lithosphere: a tool

for prediction of the age of volcanoes or oceanic crust, Geophys. J. Int. 100 (1990) 59–67.
[8] D.P. McKenzie, C. Bowin, The relationship between bathymetry and gravity in the Atlantic ocean, J. Geophys. Res. 81 (1976) 1903–1915.
[9] D. McKenzie, D. Fairhead, Estimates of the effective elastic thickness of the continental lithosphere from Bouguer and free air gravity anomalies, J. Geophys. Res. 102 (1997) 27523–27552.
[10] R.J. Banks, S.C. Francis, R.G. Hipkin, Effects of loads in the upper crust on estimates of the elastic thickness of the lithosphere, Geophys. J. Int. 145 (2001) 291–299.
[11] E. Burov, C. Jaupart, J.C. Mareschal, Large-scale crustal heterogeneities and lithospheric strength in cratons, Earth Planet. Sci. Lett. 164 (1998) 205–219.
[12] A.B. Watts, J.R. Cochran, G. Selzer, Gravity anomalies and flexure of the lithosphere: a three-dimensional study of the Great Meteor seamount, Northeast Atlantic, J. Geophys. Res. 80 (1975) 1391–1398.
[13] A. Cazenave, B. Lago, K. Dominh, K. Lambeck, On the response of the ocean lithosphere to sea-mount loads from Geos 3 satellite radar altimeter observations, Geophys. J. R. Astron. Soc. 63 (1980) 233–252.
[14] J.P. Canales, J.J. Danobeitia, The Canary Islands swell: a coherence analysis of bathymetry and gravity, Geophys. J. Int. 132 (1998) 479–488.
[15] D.L. Turcotte, L. Schubert, Geodynamics, Applications of continuum Physics to geological problems, Wiley, New York, 1982, 450 pp.
[16] R.L. Parker, The rapid calculation of potential anomalies, Geophys. J. R. Astron. Soc. 31 (1973) 447–455.
[17] C. Braitenberg, M. Zadro, Iterative 3D gravity inversion with integration of seismologic data, Boll. Geofis. Teor. Appl. 40 (1999) 469–476.
[18] C. Braitenberg, F. Pettenati, M. Zadro, Spectral and classical methods in the evaluation of Moho undulations from gravity data: the NE Italian Alps and isostasy, J. Geodyn. 23 (1997) 5–22.
[19] M. Zadro, C. Braitenberg, Spectral methods in gravity inversion: the geopotential field and its derivatives, Ann. Geofis. XL (1997) 1433–1443.
[20] C. Braitenberg, M. Zadro, J. Fang, Y. Wang, H.T. Hsu, Gravity inversion in Quinghai-Tibet plateau, Phys. Chem. Earth 25 (2000) 381–386.
[21] C. Braitenberg, M. Zadro, J. Fang, Y. Wang, H.T. Hsu, The gravity and isostatic Moho undulations in Qinghai-Tibet plateau, J. Geodyn. 30 (2000) 489–505.
[22] C. Braitenberg, R. Drigo, A crustal model from gravity inversion in Karakorum, in: Int. Symp. on Current Crustal Movement and Hazard Reduction in East Asia and South-East Asia, Wuhan, November 4–7, 1997, Symp. Proc., pp. 325–341.
[23] J. Ebbing, C. Braitenberg, H.-J. Götze, Forward and inverse modelling of gravity revealing insight into crustal structures of the Eastern Alps, Tectonophysics 337 (2001) 191–208.
[24] M. Zadro, Spectral images of the gravitational field, Manus. Geod. 11 (1986) 207–213.
[25] R.J. Blakely, Potential Theory in Gravity and Magnetic Applications, Cambridge University Press, Cambridge, 1995, 441 pp.
[26] R.J. Banks, R.L. Parker, S.P. Huestis, Isostatic compensation on a continental scale: local versus regional mechanisms, Geophys. J. R. Astron. Soc. 51 (1977) 431–452.
[27] TRANSALP Working Group, European orogenic processes research transects the Eastern Alps, EOS Trans. AGU 82/40 (2001) 453–461.
[28] W. Frisch, Tectonic progradation and plate tectonic evolution of the Alps, Tectonics 60 (1979) 11–15.
[29] H.-J. Götze, B. Meurers, S. Schmidt, P. Steinhauser, On the isostatic state of the Eastern Alps and the Central Andes – a statistical comparison, in: R.S. Harmon, C.W. Rapela (Eds.), GSA Special Paper 265 on 'Andean Magmatism and its Tectonic Setting', 1991, pp. 279–290.
[30] R.J. Lillie, M. Bielik, V. Babuška, J. Plomerová, Gravity modelling of the lithosphere in the Eastern Alpine-Western Carpathian-Pannonian Basin region, Tectonophysics 231 (1994) 215–235.
[31] A. Wagini, P. Steinhauser, B. Meurers, Isostatic residual gravity map of Austria, U.S. Geological Survey Open File Report 87–402 (1988).
[32] G.D. Karner, A.B. Watts, Gravity anomalies and flexure of the lithosphere at mountain regions, J. Geophys. Res. 88 (1983) 10449–10477.
[33] L.H. Royden, The tectonic expression slab pull at continental convergent boundaries, Tectonics 12 (1993) 303–325.
[34] B. Andewegh, S. Cloetingh, Flexure and 'unflexure' of the North Alpine German-Austrian Molasse Basin: constraints from forward tectonic modelling, in: A. Mascle, C. Puidgefabregas, H.P. Luterbacher, M. Fernandez (Eds.), Cenozoic Foreland Basins of Western Europe, Geol. Soc. Special Publ. 134, 1998, pp. 403–422.
[35] D.W. Forsyth, Subsurface loading and estimates of the flexural rigidity of continental lithosphere, J. Geophys. Res. 90 (1985) 12623–12632.
[36] A. Kirchner, H.-J. Götze, M. Schmitz, 3-D density modelling with seismic constraints in the Central Andes, Phys. Chem. Earth 21 (1996) 289–293.